Eur. Phys. J. A **22**, 461–470 (2004)
DOI 10.1140/epja/i2004-10053-5

THE EUROPEAN PHYSICAL JOURNAL A

Systematic study of structure of carbon isotopes with the antisymmetrized molecular dynamics plus generator coordinate method

G. Thiamova[1,3,a], N. Itagaki[1], T. Otsuka[1,2], and K. Ikeda[2]

[1] Department of Physics, University of Tokyo, Hongo, Tokyo 113-0033, Japan
[2] The Institute of Physical and Chemical Research (RIKEN), Wako, Saitama, 351-0198, Japan
[3] Nuclear Physics Institute, Czech Academy of Sciences, Prague-Rez, Czech Republic

Received: 2 March 2004 / Revised version: 29 May 2004 /
Published online: 11 November 2004 –
Communicated by G. Orlandini

Abstract. The structure of low-lying states of the carbon isotopes is investigated using the improved version of the Antisymmetrized Molecular Dynamics (AMD) Multi-Slater Determinant model. The theoretical method is found to be very useful to study ground-state properties of various nuclei covering light unstable nuclei. The calculations succeed to reproduce reasonably well many experimental data for the carbon isotopes ^{12}C-^{22}C such as binding energies, the energies of the 2^+_1 states in the even-even isotopes, radii and electromagnetic transition strengths. We investigate the structure change with the increasing neutron number and observe the existence of various exotic phenomena, like the development of a neutron skin and large deformations which appear in unstable nuclei. Our calculations clearly support the existence of the $N = 8$ and $N = 16$ neutron magic numbers. The role of the spin-orbit interaction in the description of the studied isotopes and in the development of cluster structures is discussed. A special approach, important for weakly bound systems, is adopted for ^{15}C. It enables us to better describe the tail of the wave function.

PACS. 21.10.Dr Binding energies and masses – 21.10.Gv Mass and neutron distributions – 21.10.Ky Electromagnetic moments – 21.60.Gx Cluster models

1 Introduction

The structure of light neutron-rich carbon nuclei is extensively studied using radioactive isotopes beams. A newly discovered magic number $N = 16$ corresponds to the driplines of the C, N, O isotopes [1,2], *e.g.* the dripline nucleus of the C isotopes is ^{22}C. The nucleus ^{15}C has been known to have a halo structure, due to the valence neutron in the s-orbit.

The situation with another possible candidate for a nucleus with halo structure, namely ^{19}C, is quite controversial. Although several experiments have been performed to explore the structure of ^{19}C, the ground-state spin of ^{19}C still remains unknown. From simple shell model considerations, the valence neutron is expected to occupy the $1d_{5/2}$ orbital. Some shell model calculations suggest a $5/2^+$ ground state with a strong contribution from a $2s_{1/2}$ neutron coupled to the 2^+ state of ^{18}C at 1.62 MeV [3]; others predict a $1/2^+$ as a ground state with a $5/2^+$ state at 50–190 keV excitation energy [4,5]. The study of the Coulomb dissociation of ^{19}C [6] supports the ground-state spin assignment of $1/2^+$ for this nucleus. If ^{19}C is really a halo nucleus, then it is natural to expect that the valence neutron will occupy the $2s_{1/2}$ orbital. However, it is already occupied in ^{15}C, then the natural explanation would be the change of the order of the $2s_{1/2}$ and $1d_{5/2}$ orbitals; while in ^{15}C the former one is lower, the $1d_{5/2}$ orbital becomes lower with increasing neutron number. On the other hand, a lowering of the $2s_{1/2}$ orbital is also possible, in analogy to the ^{11}Be case.

As pointed out in ref. [7], the experimental evidence for the ground-state spin of ^{19}C is not yet very clear. The fairly long tail of the momentum distribution is not successfully interpreted by a model assuming a simple core-plus-$2s_{1/2}$ neutron structure. Recent investigations in GANIL show some indications of the existence of a gamma decay at 200 keV for ^{19}C , from prompt gamma measurements in coincidence with ^{19}C produced by fragmentation [8]. This is the only gamma transition so far observed and it raises the following question. Are there

[a] e-mail: thiamova@tkyntm.phys.s.u-tokyo.ac.jp

more bound excited states in ^{19}C ? If so, an isomeric state might be necessary to explain the GANIL result when no prompt gamma ray other than 200 keV was observed. Further experiments are planned which would search for such an isomeric state.

In connection with the C isotopes, the main issues to be understood are the situation with ^{19}C, the change of the order of the $2s_{1/2}$ and $1d_{5/2}$ orbits and a mechanism for the appearance of the $N = 16$ neutron magic number. A possible explanation for the latter is a structure change in the C isotopes in which the spin-isospin part of the nucleon-nucleon effective interaction and the *p-sd* shell interaction play a prominent role [2].

Recent shell model calculations are another source of information about the structure of the neutron-rich carbon isotopes. Shell model calculations using two types of *p-sd* Hamiltonian were performed in ref. [3]: WBT, modeled on a set of two-body matrix elements obtained from a bare G matrix and WBP, modeled on a one-boson exchange potential which includes the one-pion exchange potential and a long-range (monopole) interaction. For ^{16}C , WBP gives spectroscopic factors $C^2S(2s_{1/2}) = 0.60$ and $C^2S(1d_{5/2}) = 1.23$ while WBT gives $C^2S(2s_{1/2}) = 0.78$ and $C^2S(1d_{5/2}) = 1.07$. The spectroscopic factors depend on the single-particle energies and, in particular, on the crossing of the single-particle energies between ^{17}O (where the $1/2^+$ is 0.87 MeV above the $5/2^+$) and ^{15}C. Both WBP and WBT interactions present a triplet of low-lying states for ^{17}C. The WBP interaction gives a $3/2^+$ ground state, in agreement with the latest experimen tal results. However, the spectroscopic factors predicted with the WBP and WBT interactions are very similar. The $3/2^+$ ground state has basically three components, the main one being $1d_{5/2} \times [(1d^2_{5/2})]_{2^+}$. This accounts for the dominant $l = 2$ knockout to the excited 2^+ state of ^{16}C. The smaller $l = 0$ component to the same state arises from a small admixture of $2s_{1/2} \times [(1d^2_{5/2})]_{2^+}$. The predicted small cross-section to the ground state of ^{16}C comes from a small admixture of the $1d_{3/2} \times [(1d^2_{5/2})]_{0^+}$ component.

The main advantage of the Antisymmetrized Molecular Dynamics (AMD) [9] approach is that it is completely free from any model assumptions such as shell model or cluster structure, axial symmetry of the system and so on. Thus it can describe the system without prejudice in the sense that no model assumption about the wave function is made in advance. In the light nuclei where both shell model and cluster structure appear, the applicability of mean field or cluster models is not assured. The AMD method, on the other hand, can describe both of them easily.

In this paper, we apply the improved version of the AMD approach and re-analyze the systematics of the C isotopes. The r.m.s. radii, binding and 2^+_1 excitation energies, proton and neutron quadrupole moments and the $B(E2, 0^+ \to 2^+)$ values are calculated and compared with the available experimental data. The agreement between the calculated and experimental data is reasonable. The details of the adopted method and the motivation for its introduction are explained in the next section.

2 Multi-Slater determinant AMD

The motivation for introducing the improved method is as follows; in previous studies it has been shown that one Slater determinant is not enough to describe a system with a well-developed halo or neutron skin structure. An attempt to improve the description by superposing several Slater determinants did not lead to substantial improvement and the computing time increased considerably.

The improved method which we adopt in this work corresponds to the combination of AMD and the Generator Coordinate Method (GCM) [10]. The initial GCM basis wave functions are constructed in such a way that they correspond to a certain value of a properly chosen physical quantity. By changing the value of this quantity, which is constrained during the cooling process, a lot of Slater determinants with different intrinsic structure are prepared. This gives a much better basis for our AMD calculations.

In this approach, the r.m.s. radius is constrained during the cooling process and afterwards a lot of Slater determinants with different intrinsic structures (corresponding to different constrained r.m.s. radii) are superposed. The mixing amplitudes of these Slater determinants are determined after the angular-momentum projection by diagonalization of the Hamiltonian matrix. This method can be regarded as a combination of projection after variation (PAV) (the preparation of the GCM basis by applying the cooling method with a constraint) and variation after projection (VAP) (GCM diagonalization with the angular momentum and parity projected wave functions). We expect that by this double variational procedure more reliable wave functions are obtained than by applying the (PAV) itself. Furthermore, when we solve the cooling equation, different initial sets of parameters are prepared to take into account many local minima of the constraint function, which will be defined later. These minima correspond to different possible geometrical arrangements of the nucleons.

First, we introduce the simple AMD method without any constraint. The total wave function ($|\Psi^{J^\pm}_{MK}\rangle$) is described as a superposition of J^π projected AMD wave functions ($|\Phi^{J^\pm}_{MK}(\boldsymbol{Z}^{n(\beta)};\beta)\rangle$) as follows:

$$|\Psi^{J^\pm}_{MK}(\boldsymbol{Z})\rangle = \sum_\beta c^\beta |\Phi^{J^\pm}_{MK}(\boldsymbol{Z}^\beta;\beta)\rangle. \tag{1}$$

Here β represents the index of an AMD basis function, and the coefficients c^β are determined by diagonalizing the Hamiltonian matrix. The parameter ($\boldsymbol{Z} = \boldsymbol{Z}_1, \ldots, \boldsymbol{Z}_A$) represents the centers of the Gaussian wave packets of nucleons. Here, the parity and the angular momentum are projected to good quantum numbers,

$$|\Phi^\pm(\boldsymbol{Z})\rangle = \hat{P}^J_{MK}\hat{P}^\pm|\Phi(\boldsymbol{Z})\rangle, \tag{2}$$

$$\hat{P}^\pm = \frac{1}{2}(1 \pm \hat{P}^{(r)}), \tag{3}$$

$$\hat{P}^J_{MK} = \int \mathrm{d}\alpha\mathrm{d}(\cos\beta)\mathrm{d}\gamma D^{J*}_{MK}(\alpha\beta\gamma)R(\Omega)\,. \tag{4}$$

Each AMD wave function in eq. (2) for the A-nucleon system has the following form:

$$|\Phi(\boldsymbol{Z}_1\ \boldsymbol{Z}_2, ..., \boldsymbol{Z}_A)\rangle = \mathcal{A}[\phi_1\phi_2\cdots\phi_A], \tag{5}$$

$$\phi_i = \psi_i\chi_i, \tag{6}$$

where ϕ_i is the i-th single-particle wave function with spatial part ψ_i and the spin-isospin part χ_i. The spatial part is expressed by a Gaussian wave packet in coordinate representation,

$$\psi_i(\boldsymbol{r}) = \left(\frac{2\nu}{\pi}\right)^{3/4} \exp\left[-\nu\left(\boldsymbol{r} - \frac{\boldsymbol{Z}_i}{\sqrt{\nu}}\right)^2 + \frac{1}{2}\boldsymbol{Z}_i^2\right], \tag{7}$$

$$\propto \exp\left[-\nu(\boldsymbol{r} - \boldsymbol{R}_i)^2 + \frac{i}{\hbar}\boldsymbol{K}_i\cdot\boldsymbol{r}\right], \tag{8}$$

where complex parameters $\boldsymbol{Z}_i = \sqrt{\nu}\boldsymbol{R}_i + \frac{i}{2\hbar\sqrt{\nu}}\ \boldsymbol{K}_i$ define the centers of the Gaussian wave packets and ν is a width parameter, that is fixed to $\nu = \frac{1}{2b^2}$, $b = 1.6$ fm. In this framework, the AMD wave functions with different intrinsic configurations corresponding to different constrained r.m.s. radii of the total system are superposed.

The diagonal elements of the Hamiltonian matrix become functions of the parameter $\boldsymbol{Z}$,

$$E(\boldsymbol{Z}, \boldsymbol{Z}^*) \equiv \frac{\langle\Phi^{\pm}(\boldsymbol{Z})|\hat{H}|\Phi^{\pm}(\boldsymbol{Z})\rangle}{\langle\Phi^{\pm}(\boldsymbol{Z})|\Phi^{\pm}(\boldsymbol{Z})\rangle}. \tag{9}$$

We optimize these parameters $\boldsymbol{Z}$ before the angular-momentum projection by using the frictional cooling method in AMD,

$$\frac{\mathrm{d}\boldsymbol{Z}_i}{\mathrm{d}\tau} = -\frac{\partial E}{\partial \boldsymbol{Z}_i^*}, \qquad \frac{\mathrm{d}\boldsymbol{Z}_i^*}{\mathrm{d}\tau} = -\frac{\partial E}{\partial \boldsymbol{Z}_i}. \tag{10}$$

As shown in ref. [9], by solving this cooling equation, the expectation value of the Hamiltonian (E) decreases with increasing imaginary time τ, since the τ derivative of E is always negative,

$$\frac{\mathrm{d}E}{\mathrm{d}\tau} = \sum_i^A \frac{\partial E}{\partial \boldsymbol{Z}_i}\cdot\frac{\mathrm{d}\boldsymbol{Z}_i}{\mathrm{d}\tau} + \sum_i^A \frac{\partial E}{\partial \boldsymbol{Z}_i^*}\cdot\frac{\mathrm{d}\boldsymbol{Z}_i^*}{\mathrm{d}\tau}, \tag{11}$$

$$= -2\sum_i^A \frac{\mathrm{d}\boldsymbol{Z}_i}{\mathrm{d}\tau}\cdot\frac{\mathrm{d}\boldsymbol{Z}_i^*}{\mathrm{d}\tau} < 0. \tag{12}$$

During this optimization of the parameters, the parity of the system is projected to a good quantum number.

As explained in the beginning of this section, one or even several Slater determinants prepared in this way are not enough to describe weakly bound systems. Some of such randomly generated Slater determinants can be basically identical after the angular-momentum projection.

Now we describe the procedure on how to prepare the AMD wave functions with an r.m.s. constraint. First we prepare several initial wave functions by solving a cooling-like equation

$$\frac{\mathrm{d}\boldsymbol{Z}_i}{\mathrm{d}\tau} = -\frac{\partial f}{\partial \boldsymbol{Z}_i^*}, \qquad \frac{\mathrm{d}\boldsymbol{Z}_i^*}{\mathrm{d}\tau} = -\frac{\partial f}{\partial \boldsymbol{Z}_i}, \tag{13}$$

where the constraint function is

$$f = (O - r^2_{\mathrm{constr.}})^2. \tag{14}$$

Here O is the expectation value of an operator $\hat{O} = \frac{1}{A}\sum_i^A r_i^2$, where r_i are the position vectors of nucleons in the center-of-mass system. The constrained values of the r.m.s. radius, $r_{\mathrm{constr.}}$, will be shown in tables 1 and 4. Values of the constraints close to the experimental r.m.s. radius are chosen as these are expected to contribute the most to the binding energy. An important point is that we prepare several wave functions with different initial parameter values for one constrained r.m.s. radius to include many local minima of the constraint function which correspond to different geometrical arrangements of the nucleons having the same r.m.s. radius.

When the value of the constraint function f is sufficiently small, we proceed to the next step. The initial wave functions correspond in general to highly excited states and are cooled down by solving the frictional cooling equation. The r.m.s. radius is kept constant during the cooling process by introducing a Lagrange multiplier in eq. (15),

$$\frac{\mathrm{d}\boldsymbol{Z}_i}{\mathrm{d}\tau} = -\frac{\partial E}{\partial \boldsymbol{Z}_i^*} + \eta\frac{\partial O}{\partial \boldsymbol{Z}_i^*}, \quad \frac{\mathrm{d}\boldsymbol{Z}_i^*}{\mathrm{d}\tau} = -\frac{\partial E}{\partial \boldsymbol{Z}_i} + \eta\frac{\partial O}{\partial \boldsymbol{Z}_i}, \tag{15}$$

Here, the multiplier η is determined by the condition that the τ derivative of O is zero,

$$\frac{\partial O}{\partial \boldsymbol{\tau}} = \sum_i^A \frac{\partial O}{\partial \boldsymbol{Z}_i}\frac{\partial \boldsymbol{Z}_i}{\partial \boldsymbol{\tau}} + \text{ c.c.},$$

$$= \sum_i^A \frac{\partial O}{\partial \boldsymbol{Z}_i}\left\{-\frac{\partial E}{\partial \boldsymbol{Z}_i^*} + \eta\frac{\partial O}{\partial \boldsymbol{Z}_i^*}\right\} + \text{ c.c.} = 0. \tag{16}$$

Therefore, the η value is determined from this equation,

$$\eta = \frac{\sum_i^A \frac{\partial O}{\partial \boldsymbol{Z}_i}\frac{\partial E}{\partial \boldsymbol{Z}_i^*} + \text{ c.c.}}{\sum_i^A \frac{\partial O}{\partial \boldsymbol{Z}_i}\frac{\partial O}{\partial \boldsymbol{Z}_i^*} + \text{ c.c.}}. \tag{17}$$

The Hamiltonian and the effective nucleon-nucleon interaction used is the same as in ref. [11]; the Majorana parameter M of the Volkov No. 2 interaction and the strength of the G3RS spin-orbit interaction are determined by the α-α and α-n scattering phase shift analyses. The strength of the Bartlett and Heisenberg terms of the central interaction has been set to zero.

We want to stress that the study of effective interactions in the AMD model is of importance because it is still not obvious which of the effective interaction parameters should be adopted in the AMD framework. The Volkov and modified Volkov interactions, although used in most existing structure AMD studies, are not global. Rather, some of the parameters have to be optimized for each region of the nuclear mass. In ref. [12], the Gogny and Skyrme SIII interactions are used to calculate ground-state properties of light nuclei. The Gogny force gives in

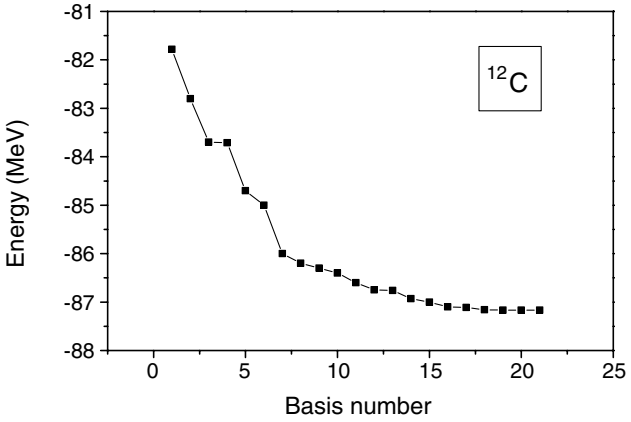

Fig. 1. Dependence of the binding energy on the number of basis functions. The first basis function is prepared without any constraint. To this basis function other basis functions are added which correspond to the r.m.s. constraints 2.225 fm to 2.700 fm with a step of 0.025 fm.

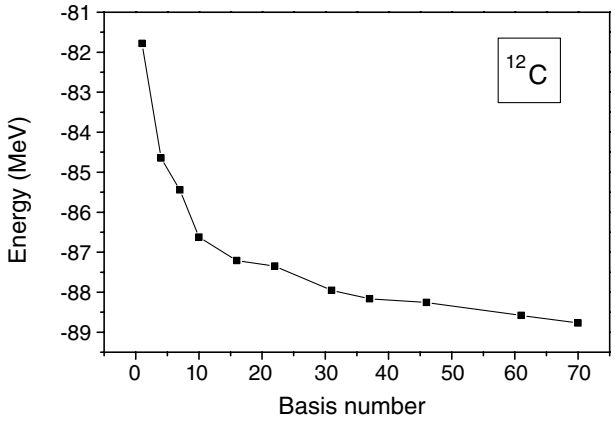

Fig. 2. Dependence of the binding energy on the number of basis functions. Three r.m.s. constraints 2.3, 2.4 and 2.5 fm are kept constant and for each of them 1 up to 23 basis functions are prepared.

general slightly better results than the SIII force, but the tendency is similar for both interactions. Structure of light unstable Li, Be, B and C isotopes using Volkov No. 1 and Case (1) and Case (3) of the modified MV1 interactions containing the zero-range three-body force as a density-dependent term is investigated in ref. [13].

3 Results

First, we show the results for the even-even C isotopes.The number of basis states employed are summarized in table 1. For each constrained value of the r.m.s. radius $r_{\mathrm{constr.}}$, 15 basis states calculated from different initial parameter sets are prepared. Obviously, the binding energies are also improved by a superposition of a larger number of basis states. For a comparison, when only three basis wave functions are taken for ^{16}C (one for each $r_{\mathrm{constr.}}$= 2.3, 2.4 and 2.5 fm in table 1), the calculated ground-state binding energy is about 5 MeV lower than when 45 basis functions are adopted (15 basis functions for the same $r_{\mathrm{constr.}}$).

In fig. 1 the dependence of the binding energy of ^{12}C on the number of basis functions is shown. Here, 1 on the horizontal axis corresponds to one basis function, which is calculated without any constraint. And 2 on the horizontal axis shows the superposition of this basis function and one whose r.m.s. radius is constrained to $r_{\mathrm{constr.}}$ = 2.225 fm. Then 3 corresponds to the superposition of these two basis functions and a new one with $r_{\mathrm{constr.}}$ = 2.250 fm and so on up to $r_{\mathrm{constr.}}$ = 2.700 fm with a step of 0.025 fm. As is seen from the figure, when the convergence is reached, the binding energy is still much smaller than the experimental value of 92.2 MeV.

In fig. 2 a different type of convergence of the binding energy of ^{12}C as a function of the total number of basis functions is shown. Here, three different constraints $r_{\mathrm{constr.}}$ = 2.3, 2.4 and 2.5 fm are kept fixed and only the number of basis functions generated for each of them changes. Thus, for example, 69 basis functions means 23 basis functions for each $r_{\mathrm{constr.}}$. Even though the convergence is worst, it is seen that a better approximation of the binding energy can be reached. We want to stress that the fact that the binding energy is still smaller than the experimental one is due to a specific character of the ground state of ^{12}C as will be discussed later.

Table 1. The number of the employed basis states for the even-even C isotopes as a function of constrained r.m.s. radius. 15 basis states calculated from different initial parameter sets are prepared for each constrained value of the r.m.s. radius.

$r_{\mathrm{constr.}}$ (fm)	^{12}C	^{14}C	^{16}C	^{18}C	^{20}C	^{22}C
2.3	15					
2.4	15	15				
2.5	15	15	15			
2.6		15	15	15	15	
2.7			15	15	15	15
2.8				15	15	15
2.9						15

Calculations with a huge number of basis functions renders the systematic calculations extremely time consuming. This is why we use a smaller number of basis functions (45 for the even-even and 60 for the even-odd isotopes), but large enough to obtain reasonable values of the calculated quantities. Furthermore, we have checked that when the number of basis functions is further increased, the calculated quantities already do not change much. For example, when 60 basis functions are used for ^{12}C, the $B(E2, 0^+ \rightarrow 2^+)$ value, the proton Q_{p} and neutron Q_{n} quadrupole moments of the 2_1^+ state and the expectation value of the harmonic-oscillator quanta $\langle \hat{N} \rangle$ are 21.70 e^{2}fm^4, 2.48 fm^2, 2.40 fm^2 and 8.27, respectively, which are basically the same values as those obtained with 45 basis functions for (see table 2).

The calculated quantities and the available experimental data for the even-even isotopes are presented in figs. 3-7 and the numerical values are shown in table 2.

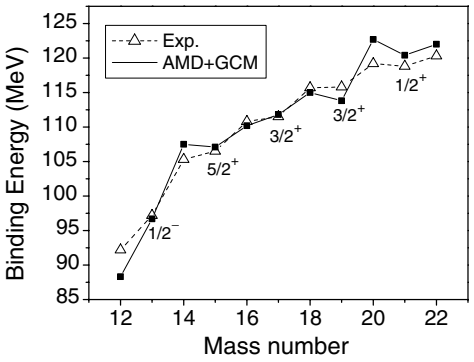

Fig. 3. Experimental (open triangles) and calculated (squares) binding energies of ^{12}C-^{22}C.

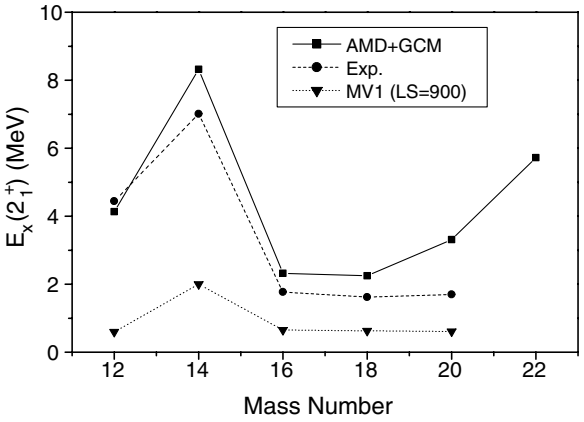

Fig. 4. Experimental (circles) and calculated (squares) energies of the 2_1^+ states of the even-even carbon isotopes. A comparison is made with the calculation from ref. [13] (triangles).

The calculated binding energy of ^{12}C is smaller than the experimental value (fig. 3). This may be partially due to the adopted value of the width parameter ν, which is kept fixed for all isotopes. Since the 3α-like component is important in the ground-state wave function of ^{12}C, larger value of ν, closer to the α-particle value, could be adopted and the binding energy would increase. To tune the parameter ν to the binding energy is, of course, possible but we would have obtained an effective value of ν, influenced, in general, by the chosen effective interaction and the model space. We will not do it in a systematic way because the Volkov interaction itself is known to give insufficient binding energy for ^{12}C when the Majorana parameter has value $M = 0.6$, a value adopted to fit the binding energy of ^{16}O and there are also indications that the adopted spin-orbit interaction is too strong. We will, however, document the dependence of the binding energy on the width parameter by a simple calculation shown in table 3 and explained in the next paragraph.

The width parameter ν is fixed to be the same for all single-particle wave functions. In this way, we can remove the spurious center-of-mass motion exactly from the Hamiltonian. It is also fixed to be the same for all studied isotopes. Thus, the basis states used in this paper represent minima under the constraint of the fixed width parameter. Its value is reasonable for heavier isotopes, but the case of ^{12}C deserves more attention due to the special character of its ground state. The ground state of ^{12}C has a transient character between shell model and 3α-cluster structure. By a simple calculation we may document how its binding energy changes when different width parameters are adopted and when an $S = 1$ component of a two-particle wave function is explicitly taken into account by choosing spin-up projections for one proton and one neutron (thus having $S_z = 1$). In table 3 the calculations with one basis wave function corresponds to total spin projection $S_z = 0$. The binding energy becomes larger when ν approaches the α-particle value 0.23 fm^{-2}. When we perform a large-scale calculation with 45 basis functions and $\nu = 0.23$ fm^{-2}, the binding energy $E_{\rm bin} = 93$ MeV, close to the experimental value. We do not observe a clear minimum of the binding energy when varying ν, but we can at least adjust its value to fit the binding energy of ^{12}C. We believe that the fact that the adjusted value is close to the α-particle value reflects the 3α-cluster component of the ^{12}C ground state.

By including the $S_z = 1$ component, the binding energy further decreases. So this component may be important. However, this effect is already included in our large-scale calculations, because all two-particle configurations occupying time-reversal orbits and having spin $S = 0$ will also have $S = 1$ (even if $S_z = 0$). Furthermore, the case of the ^{12}C isotope is a special one and the spin-orbit interaction acts strongly.

The ^{12}C and ^{14}C nuclei correspond to neutron subclosed ($N = 6$) and closed ($N = 8$) shells, respectively, and both the calculated and experimental 2_1^+ energies are rather high (fig. 4). However, the calculated 2_1^+ energy of ^{14}C (8.32 MeV) is higher than the experimental value (7.01 MeV). One of the reasons for this is most probably the larger spin-orbit splitting of the $1p_{1/2}$ and $1p_{3/2}$ spin-orbit partners which brings the dominant proton configuration $(1p_{3/2})^3(1p_{1/2})^1$ higher in energy. Support for this argument comes also from a higher $3/2^-$ state (6.49 MeV) than the experimental value (3.68 MeV) in ^{13}C (fig. 8a).

On the other hand, the spin-orbit interaction plays an important role in describing the 2_1^+ state in ^{12}C. In the cluster model calculations the level spacing between the 0_1^+ and 2_1^+ states was always underestimated. For instance, in a GCM calculation [14] it was 2.2 MeV, which is much smaller than the experimental value 4.4 MeV. In the present approach this level spacing is well reproduced, and it is because the theory describes the dissociation of the α cluster in the ground state 0_1^+ due to the LS force [15]. Also, in ref. [13] a systematic study of carbon isotopes is performed, using several sets of effective interactions with much weaker spin-orbit term (900 and 1500 MeV) and the 2_1^+ energies are systematically much smaller than the experimental ones (fig. 4). Thus, it seems that the choice of a proper effective interaction with a spin-orbit term is a key issue in the study of carbon isotopes and needs further investigation.

Table 2. The calculated binding energies (B.E.), the excitation energies of the 2_1^+ states (E_x (2^+)) and the radii (r) of the even-even isotopes. The values in parenthesis are the experimental data. The experimental r.m.s. values are deduced from the interaction cross-section using the Glauber model [16]. In the last five rows are the $B(E2, 0^+ \to 2^+)$ values, the proton Q_p and neutron Q_n quadrupole moments of the 2_1^+ states, the expectation values for the total number of the oscillator quanta $\langle\hat{N}\rangle$ and its shell model limit.

	^{12}C	^{14}C	^{16}C	^{18}C	^{20}C	^{22}C
B.E. (MeV)	88.3 (92.2)	107.5 (105.3)	110.2 (110.8)	115.0 (115.7)	122.7 (119.2)	122.0 (120.3)
E_x (2^+) (MeV)	4.13 (4.44)	8.32 (7.01)	2.32 (1.77)	2.25 (1.62)	3.31 (1.70)	5.72
r (fm)	2.40 (2.35±0.02)	2.39 (2.30±0.07)	2.55 (2.70±0.03)	2.65 (2.82±0.04)	2.65 (2.98±0.05)	2.79
$B(E2, 0^+ \to 2^+)$(e^{2}fm^4)	21.69 (41 ± 5)	25.84 (18.7 ± 2.5)	7.62 (3.1 ± 0.02)	5.29	13.93	4.03
$Q_\mathrm{p}(2_1^+)$ (fm^2)	7.80	8.60	−1.74	−3.65	6.21	−1.49
$Q_\mathrm{n}(2_1^+)$ (fm^2)	7.64	2.54	−13.85	−20.29	18.80	−13.06
$\langle\hat{N}\rangle$	8.27	10.22	14.25	18.35	22.21	26.36
$\langle\hat{N}\rangle$ (shell model limit)	8	10	14	18	22	26

Table 3. Binding energies (in MeV) for ^{12}C as a function of the width parameter $\nu = 1/2b^2$ fm^{-2}. In the first row, calculations with one basis function are presented ($S_z = 0$). In the second row, calculations with 3 basis functions ($S_z = 1$) are shown.

	$b = 1.4$	$b = 1.5$	$b = 1.6$	$b = 1.7$
1 b.f.	89.62	85.19	81.78	77.30
3 b.f.	95.80	90.89	85.75	80.09

The overbinding observed for ^{20}C and ^{22}C (fig. 3) can be also partially attributed to the used spin-orbit interaction. Furthermore, we observe an increase of the 2_1^+ energy in ^{20}C. Our calculation thus suggests a $(1d_{5/2})^6$ sub-shell closure, not observed in the experimental data. On the contrary, the experimental values of the 2_1^+ energies of ^{16}C, ^{18}C and ^{20}C are almost the same, suggesting the $2s_{1/2}$ and $1d_{5/2}$ orbits are almost degenerate in these isotopes. In our case, the large spin-orbit splitting of the $1d_{5/2}$ and $1d_{3/2}$ orbits brings the $1d_{5/2}$ orbit lower in energy and the sub-shell closure may develop. This effect may be partially responsible for the fact that the calculated spin of the ground state of ^{15}C is $5/2^+$ instead of $1/2^+$, as will be shown later.

The experimental 2_1^+ energy of ^{22}C is not known yet. In our calculation a high value (5.7 MeV) is obtained (fig. 4). If this sharp increase at ^{22}C is measured, this would be a strong evidence for the $N = 16$ neutron magic number. Although the calculated values of the r.m.s. radii are relatively smaller than the experimental ones, both show drastic increase at ^{16}C (fig. 5). This kink of the r.m.s. radius is mainly due to the fact that two valence neutrons are added to the *sd*-shell. The radii are known to be sensitive to the value of the Majorana parameter M. Larger values of M can be adopted for heavier isotopes which would lead to slightly larger radii. In our calculations, this parameter has been kept constant at $M = 0.6$ over the whole isotope region for the sake of simplicity. We expect that systematically larger radii can be obtained when a density-dependent interaction is used because r.m.s. radii are also sensitively dependent on it. On the other hand, the experimental r.m.s. radii may be model dependent and not so precise as they are derived indirectly using the Glauber theory. As can be seen from fig. 5, the radii become larger and larger in the region heavier than ^{14}C. This is mainly due to the fact that the neutron radii become larger due to the development of the neutron skin structure (another evidence comes from the neutron quadrupole moments, as will be shown later) while the proton radii are more stable with the increase of the neutron number, similarly to the results in ref. [13].

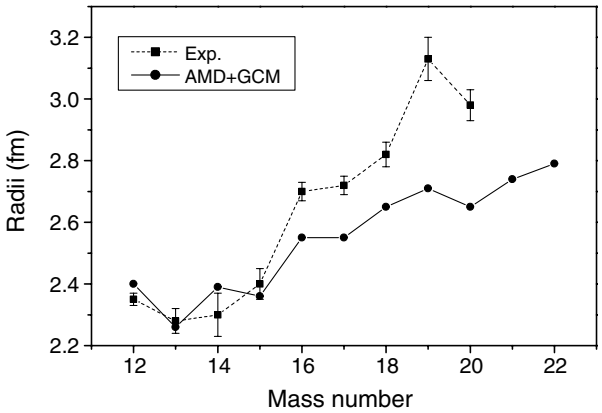

Fig. 5. Comparison of the experimental (squares) and calculated (circles) r.m.s. radii for ^{12}C-^{22}C. The experimental values are deduced from the interaction cross-sections using the Glauber model.

In order to analyze the development of clustering quantitatively, we calculate the expectation value of the operator of the total number of the oscillator quanta $\hat{N} = \sum_i \hat{a}_i^\dagger \hat{a}_i$, where $\hat{a}_i^\dagger$, $\hat{a}_i$ are the creation and annihilation

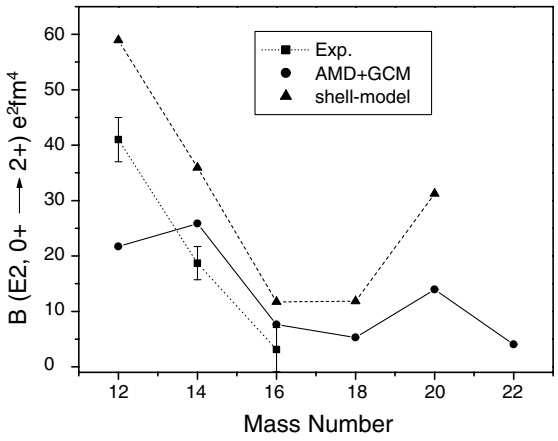

Fig. 6. Experimental (squares) and calculated (circles) $B(E2)$ transition strengths for the even-even carbon isotopes. Comparison is made with a shell model calculation using effective charges (triangles).

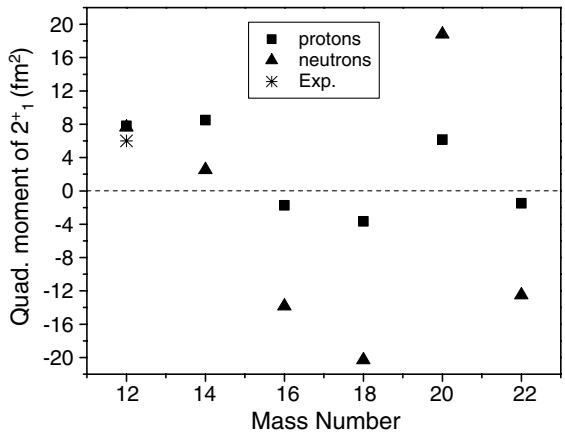

Fig. 7. Calculated laboratory quadrupole moments for protons (squares) and neutrons (triangles) for the even-even carbon isotopes. The experimental value for ^{12}C is indicated by an asterix.

operators of harmonic-oscillator quanta, respectively. In general, if the clustering is developed, the wave function of the system contains the components of many orbits in higher shells and the expectation value of the oscillator quanta is large. On the other hand, a small value of the oscillator quantum number indicates that the state is close to the shell model one in the $0\hbar\omega$ configuration and the spatial clustering is not developed. Our values of $\langle\hat{N}\rangle$ are close to the shell model limit for all isotopes. For ^{14}C and heavier isotopes, this is what should be expected because the clustering structure dissapears in neutron-rich carbon isotopes. The small deviation from the shell model lower limit value for the heavier isotopes is due to the contribution of many neutrons. A larger value of $\langle\hat{N}\rangle$ for ^{12}C should be obtained when the 3α component of the ground-state wave function of ^{12}C is taken into account effectively. Later we will show how $\langle\hat{N}\rangle$ and other quantities change, when the spin-orbit interaction, which suppresses the development of a cluster structure, is decreased.

The comparison of experimental $B(E2)$ values with those calculated within the shell model [17] and in the present approach are shown in fig. 6. The calculated $B(E2)$ value for ^{12}C is smaller than the experimental value. This is most probably due to the small amplitude of the 3α component in the ground-state wave function. The $B(E2)$ values for the ^{16}C and ^{18}C isotopes are very small. As is discussed in ref. [17], the neutron effective charges become very small in the nuclei where neutrons are weakly bound. In ^{16}C almost all contributions to the $B(E2)$ value comes from neutrons because the protons form an almost closed shell model configuration. Thus, the reduction of the neutron effective charges affects the $B(E2)$ value strongly. Namely, the reduction of the neutron effective charge for the transition between the $2s_{1/2}$ and $1d_{5/2}$ orbits is of particular importance, because the ground state of ^{16}C contains a large $(2s_{1/2})^2(\nu)$ component. A similar mechanism makes the $B(E2)$ value small for ^{18}C. The $B(E2)$ value for ^{16}C has been measured recently [18] and it is indeed very small. In ^{20}C, the proton contribution to the $B(E2)$ values becomes again larger, because the contribution of protons increases. In general, the results we have obtained within the AMD method with bare charges are in a good qualitative agreement with those obtained within the above-mentioned shell model calculation and in reasonable agreement with the experimental data.

The quadrupole moment of protons $Q_{\rm p}$ of ^{16}C is much smaller than $Q_{\rm n}$, as should be expected for a closed shell proton configuration (fig. 7). The same is true also for ^{18}C. A slight increase of $Q_{\rm p}$ is observed in ^{20}C. The quadrupole moments $Q_{\rm p}$ and $Q_{\rm n}$ are almost the same in ^{12}C, while $Q_{\rm n}$ decreases significantly in ^{14}C with the neutron magic number $N = 8$. Again, we would expect larger values for ^{12}C if the 3α component were stronger in the ground-state wave function. In the next paragraph we will show how the calculated quantities change when the spin-orbit term, which governs the development of the cluster structure, is decreased. We may notice much larger absolute values of the neutron quadrupole moments relative to the proton quadrupole moments in the neutron-rich region, which shows that the neutron density in the neutron-rich region reaches widely into the outer region. We also recall that in ref. [19], where the Skyrme SIII case interaction is employed in an AMD calculation without angular-momentum projection, the proton deformation of ^{16}C and ^{18}C is prolate. Protons of these nuclei then would be separated into two spatial parts. On one side, there are two protons, and on the other side, there are four protons. The Hartree-Fock calculations with the Gogny force [20] and with the Skyrme SIII force [21] also give prolate proton deformations for ^{16}C and ^{18}C. However, the results of the AMD calculation with the MV1 force [22] contradict these results, suggesting, that protons of the carbon isotopes are all oblately deformed. From all these results it seems that the proton deformations of ^{16}C and ^{18}C are more sensitive to the effective interaction. We would like to stress another interesting feature observed in our calculation, namely that the proton distribution seems to adjust its

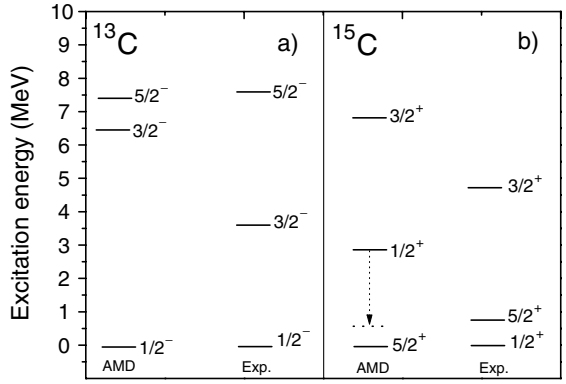

Fig. 8. Excitation energies of the lowest negative-parity states for ^{13}C are compared with the experimental levels in a). In b) the experimental and calculated energies of the lowest positive-parity states in ^{15}C are compared. The dotted line indicates the energy of the $1/2^+$ state obtained with the angular-momentum projection + relative orientation method.

deformation to the neutron one, to increase the overlap of the proton and neutron matter distribution. This may show the importance of the proton-neutron interaction in neutron-rich nuclei.

Now we want to show how the $B(E2, 0^+ \to 2^+)$ values, quadrupole moments and the expectation values of the harmonic-oscillator quanta $\langle\hat{N}\rangle$ change when the spin-orbit interaction is artificially decreased. It is known that the spin-orbit interaction acts against the development of spin-isospin saturated clusters, such as the α particles, because in such clusters $S = 0$ and the spin-orbit interaction cannot contribute. Thus, by weakening the spin-orbit interaction, a cluster component of a wave function should increase, which should be reflected in the above-mentioned quantities. We have decreased the absolute value of the strength of both terms in the two-range G3RS spin-orbit interaction from the original value of 2000 MeV to 1750 MeV, 1500 MeV and 1200 MeV. In the first case, $B(E2, 0^+ \to 2^+)$, $Q_{\rm p}$, $Q_{\rm n}$ and $\langle\hat{N}\rangle$ are 24.0 e^{2}fm^4, 2.69 fm^2, 2.60 fm^2 and 8.31, respectively, and in the second case, the same quantities have the values 26.0 e^{2}fm^4, 2.83 fm^2, 2.77 fm^2 and 8.36, respectively. In the last case, they are 28.91 e^{2}fm^4, 2.97 fm^2, 2.90 fm^2 and 8.43, respectively. Increase of all the quantities indicates increase of the deformation and development of the spatial clustering. This also demonstrates the importance of a properly chosen effective interaction for the description of the experimental data.

Next we discuss the even-odd C isotopes; the number of basis states for each isotope is shown in table 4. The calculated and experimental binding energies and r.m.s. radii are presented in figs. 3 and 5. The numerical values are shown in table 5.

Agreement of the calculated and experimental binding energies is reasonable. However, the ground-state spin and the halo structure of the ^{15}C nucleus are not reproduced and the excitation energy of the $1/2^+$ state in the ^{19}C nucleus is relatively high (figs. 8b, 9b). We have to remember

Table 4. The number of the employed basis states for the even-odd C isotopes as a function of constrained r.m.s. radius.

$r_{\rm constr.}$ (fm)	^{13}C	^{15}C	^{17}C	^{19}C	^{21}C
2.3	30				
2.4	30	30			
2.5		30			
2.6			30		
2.7			30	10	
2.8				10	30
2.9				10	30
3.0				10	
3.1				10	
3.2				10	

that the ground-state properties of ^{19}C are not very well known experimentally. It is possible that the large interaction cross-section from which the large r.m.s. radius has been extracted is due to the presence of an isomeric state, as suggested by the measurements in GANIL [8].

Shell model calculations performed in ref. [3] show there is a triplet of low-lying $1/2^+$, $3/2^+$ and $5/2^+$ states in ^{17}C, with ordering dependent on the used interaction. However, the latest experiments favor a $3/2^+$ as a ground state [23], which is reproduced by our model (fig. 9a).

In ^{15}C the $2s_{1/2}$ orbital is below the $1d_{5/2}$ orbital. This fact is clearly observed as an abnormal ground-state spin parity $J^\pi = 1/2^+$ of this nucleus. The lowering of the s orbital is due to the halo formation. The halo is formed since the orbital with lowest angular momentum gains energy by extending its wave function. For ^{15}C we did not obtain the ground-state spin $1/2^+$. Our calculation gives -104.2 MeV for the $1/2^+$ state and -107.1 MeV for the $5/2^+$ state (fig. 8b). The fact that the $5/2^+$ state is lowest may be also given by stronger spin-orbit interaction which brings the $1d_{5/2}$ orbit down in energy. In ref. [9], where the MV1 force with a density-dependent term is used to calculate the magnetic moments of the carbon isotopes, the ground-state spin $1/2^+$ of ^{15}C is not reproduced either. This may also show the limitation of the AMD approach which may be too simple for the description of the exotic, neutron-rich nuclei.

To describe the tail of the wave function next we adopt a projection + multiple relative orientation (between the core and the valence neutron) technique. If we only project the total J^π of ^{15}C, the wave function describing the relative motion of the valence neutron and ^{14}C is not optimized, and we cannot obtain correct ordering of the levels. Therefore, this new technique is necessary, especially for the weakly bound systems with deformed cores. We express this effect by superposing single projected wave functions. First, the core wave functions (^{14}C) are generated and afterwards on each of them several wave functions of the last valence neutron are superposed, each of them corresponds to a different relative orientation with respect to the core. If the basis states of ^{14}C correspond to the r.m.s. constraint 2.3, 2.4 and 2.5 fm (only one basis state for each r.m.s. radius) and for each of them 16 basis states are superposed, the $1/2^+$ state is about 1 MeV

Table 5. The calculated binding energies (B.E.) and radii (r) of the even-odd isotopes. The spin and parity of the lowest state which come out from the calculations is also indicated. The values in parenthesis are the experimental data. The experimental values for the radii are deduced from the interaction cross-section using the Glauber model [16].

	^{13}C	^{15}C	^{17}C	^{19}C	^{21}C
J^π(cal.)	$1/2^-$	$5/2^+$	$3/2^+$	$3/2^+$	$1/2^+$
B.E. (MeV)	96.7 (97.2)	107.1 (106.5)	111.8 (111.5)	113.8 (115.8)	120.4 (118.8)
r (fm)	2.26 (2.28±0.04)	2.36 (2.40±0.05)	2.55 (2.72±0.03)	2.71 (3.13±0.07)	2.74

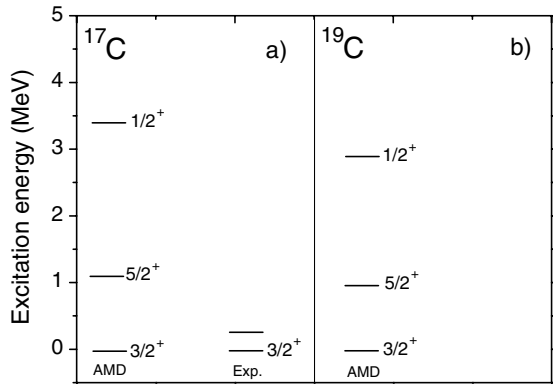

Fig. 9. The lowest positive-parity states in ^{17}C are compared with the experimental levels in a). In b) the lowest positive-parity levels for ^{19}C are shown.

higher than $5/2^+$, which is much less than in the original calculation where this energy difference is typically several MeV. When a larger number of basis wave functions is adopted (5 wave functions for 3 different r.m.s. constraints for ^{14}C and for each of them 10 wave functions for the valence neutron), the $1/2^+$ state is 0.6 MeV above $5/2^+$ (the dotted line in fig. 8b).

The lowest normal parity states of ^{19}C are displayed in fig. 9b. The basis states with large r.m.s. radii are employed in an attempt to reproduce the suggested large r.m.s. radius (see table 4). The obtained energies are -110.9 MeV, -113.8 MeV, and -112.8 MeV for the $1/2^+$, $3/2^+$, and $5/2^+$ states, respectively. In general, in all calculations we have performed (with different number of basis wave functions, r.m.s. constraints, strength of the spin-orbit interaction) the energies of the first $1/2^+$, $3/2^+$ and $5/2^+$ states are close to each other and in some of them the $5/2^+$ state is lowest. The variation of the spin-orbit strength affects also the $1/2^+$ state which shows that this state has a Nilsson-like character in this model. We recall that similar results have been obtained also in ref. [3], where shell model calculations led to a triplet of low-lying levels with spin-parity $1/2^+$, $3/2^+$ and $5/2^+$ and their ordering depended on the adopted effective interaction, similarly to ^{17}C. It is considered that the $1/2^+$ state can be pulled down by applying the same technique as the one adopted for ^{15}C. We can conclude that the idea of a valence neutron in the s-orbit used to explain the large r.m.s. radius of ^{19}C is not supported by our calculation.

In general, the strongly repulsive $1p_{3/2}(\pi)$-$1d_{5/2}(\nu)$ tensor interactions [2], would be partially responsible for the crossing of the $1d_{5/2}$ and $2s_{1/2}$ orbits in the carbon isotopes. This effect is not included in our model. A proper description of the pairing interaction between neutrons on the $1d_{5/2}$ orbital is also important. On the other hand, the lowering of the $2s_{1/2}$ single-particle energy coming from the decrease of the kinetic energy can be described by the above-mentioned technique, as done for ^{15}C. However, as has been stressed at the beginning, the situation with the ground state of ^{19}C is still unclear and awaits further experimental investigations.

4 Conclusion

In this paper we have presented systematic calculations for ^{12}C-^{22}C. Large number of quantities have been calculated for the even-even isotopes. The calculated binding energies are in reasonable agreement with the experimental data. The systematic comparison of the binding and 2_1^+ energies of the even-even isotopes with the experimental data reveals the importance of the spin-orbit term of the effective interaction. Specifically, the calculated energy of the 2_1^+ state in ^{14}C and the observed sub-shell closure in ^{20}C suggest the spin-orbit term should be weaker. On the other hand, with a weaker spin-orbit interaction the energy of the 2_1^+ state in ^{12}C is much lower than the experimental value. It seems that this point deserves more detailed investigation. The neutron magic number $N = 8$ is reflected by the large 2_1^+ energy of ^{14}C. A very large 2_1^+ energy of ^{22}C supports the idea of an $N = 16$ neutron magic number.

The r.m.s radii systematically increase beyond ^{14}C. This can be explained by the development of a neutron skin. This fact is reflected also by the neutron quadrupole moments, which increase beyond ^{14}C, indicating the neutron matter distribution stretches widely in the outer region. An interesting tendency is observed in the behaviour of the proton deformation which seems to adapt to that of the neutrons.

The calculated $B(E2)$ values show a behavior similar to that obtained by shell model calculations with reduced effective neutron charges. The advantage of the AMD method is that no effective charges have to be used, because the changes of neutron and proton distribution are authomatically described by the model. A recently

measured very small $B(E2)$ value for ^{16}C is successfully reproduced by our model.

The calculated binding energies for the even-odd isotopes are in good agreement with the experimental values. The ground-state spin of ^{17}C is reproduced. For the ^{15}C isotope, a good description of the tail of the wave function is important. It has been achieved by applying a projection + multiple relative orientation technique and a much lower $1/2^+$ state has been obtained. The situation with the ground-state spin of ^{19}C is unclear and further experiments are necesssary to solve the controversial predictions from the previous experiments.

One of the authors (N.I.) thanks Prof. H. Horiuchi and Dr. Y. Kanada-En'yo for fruitful discussions. G.T. is indebted to Dr. P. Cejnar and Prof. D.J. Rowe for careful reading of the manuscript and dedicates this paper to Dr. Milena Serra, colleague and friend, who died so unexpectedly. This work is supported in part by Grant-in-Aid for Scientific Research (13740145) from the Ministry of Education, Science and Culture. The financial support from the Japanese Society for Promotion of Science under the grant No. P01769 is acknowledged.

References

1. A. Ozawa, T. Kobayashi, T. Suzuki, K. Yoshida, I. Tanihata, Phys. Rev. Lett. **84**, 5493 (2000).
2. T. Otsuka, R. Fujimoto, Y. Utsuno, B.A. Brown, M. Honma, T. Mizusaki, Phys. Rev. Lett. **87**, 082502 (2001).
3. V. Maddalena *et al.*, Phys. Rev. C **63**, 024613 (2001).
4. D. Bazin *et al.*, Phys. Rev. Lett. **74**, 3569 (1995).
5. E.K. Warburton, B.A. Brown, Phys. Rev. C **46**, 923 (1992).
6. T. Nakamura *et al.*, Phys. Rev. Lett. **83**, 1112 (1999).
7. R. Kanungo *et al.*, Nucl. Phys. A **677**, 171 (2000).
8. GANIL, private comunication.
9. Y. Kanada-En'yo, H. Horiuchi, Phys. Rev. C **54**, R468 (1996).
10. N. Itagaki, S. Aoyama, Phys. Rev. C **61**, 024303 (2000).
11. N. Itagaki, S. Okabe, Phys. Rev. C **61**, 044306 (2000).
12. Y. Sugawa, M. Kimura, H. Horiuchi, Prog. Theor. Phys. Suppl. **106**, 1129 (2001).
13. Y. Kanada-En'yo, H. Horiuchi, Prog. Theor. Phys. Suppl. **142**, 205 (2001).
14. E. Uegaki, S. Okabe, Y. Abe, H. Tanaka, Prog. Theor. Phys. **57**, 1262 (1977); E. Uegaki, Y. Abe, S. Okabe, H. Tanaka, Prog. Theor. Phys. **59**, 1031 (1978); **62**, 1621 (1979).
15. Y. Kanada-En'yo , Phys. Rev. Lett. **81**, 5291 (1998).
16. A. Ozawa, T. Suzuki, I. Tanihata, Nucl. Phys. A **693**, 33 (2001).
17. R. Fujimoto, PhD Thesis, University of Tokyo (2002).
18. N. Imai, Z. Elekes, private communication.
19. M. Kimura, Y. Sugawa, H. Horiuchi, Prog. Theor. Phys. **106**, 1153 (2001).
20. R. Blumel, K. Dietrich, Nucl. Phys. A **471**, 453, (1987).
21. N. Tajima, S. Takahara, N. Onishi, Nucl. Phys. A **603**, 23 (1996).
22. Y. Kanada-En'yo, H. Horiuchi, A. Ono, Phys. Rev. C **52**, 628 (1995).
23. K. Asahi *et al.*, Nucl. Phys. A **704**, 88c (2002).